RESEARCH ARTICLE

A new look at ocean carbon remineralization for estimating deepwater sequestration

Lionel Guidi[1,2], Louis Legendre[1], Gabriel Reygondeau[3,4], Julia Uitz[1], Lars Stemmann[1], and Stephanie A. Henson[5]

[1]Sorbonne Universités, UPMC Université Paris 06, CNRS, Laboratoire d'oceanographie de Villefranche (LOV), Observatoire Océanologique, Villefranche-sur-Mer, France, [2]Department of Oceanography, University of Hawaii, Honolulu, Hawaii, USA, [3]Center for Macroecology, Evolution and Climate, National Institute for Aquatic Resources, Technical University of Denmark (DTU Aqua), Charlottenlund, Denmark, [4]Fisheries Centre, University of British Columbia, Aquatic Ecosystems Research Laboratory, Vancouver, Canada, [5]National Oceanography Centre, European Way, Southampton, UK

Abstract The "biological carbon pump" causes carbon sequestration in deep waters by downward transfer of organic matter, mostly as particles. This mechanism depends to a great extent on the uptake of CO_2 by marine plankton in surface waters and subsequent sinking of particulate organic carbon (POC) through the water column. Most of the sinking POC is remineralized during its downward transit, and modest changes in remineralization have substantial feedback on atmospheric CO_2 concentrations, but little is known about global variability in remineralization. Here we assess this variability based on modern underwater particle imaging combined with field POC flux data and discuss the potential sources of variations. We show a significant relationship between remineralization and the size structure of the phytoplankton assemblage. We obtain the first regionalized estimates of remineralization in biogeochemical provinces, where these estimates range between −50 and +100% of the commonly used globally uniform remineralization value. We apply the regionalized values to satellite-derived estimates of upper ocean POC export to calculate regionalized and ocean-wide deep carbon fluxes and sequestration. The resulting value of global organic carbon sequestration at 2000 m is 0.33 Pg C yr^{-1}, and 0.72 Pg C yr^{-1} at the depth of the top of the permanent pycnocline, which is up to 3 times higher than the value resulting from the commonly used approach based on uniform remineralization and constant sequestration depth. These results stress that variable remineralization and sequestration depth should be used to model ocean carbon sequestration and feedback on the atmosphere.

1. Introduction

The "biological carbon pump" leads to carbon sequestration by vertical transfer to depth of some of the organic carbon that results from phytoplankton photosynthesis in the upper ocean. Carbon is said to be sequestered when it cannot return to the atmosphere for at least 100 years or when it reaches depths >1000 m [*Lampitt et al.*, 2008; *Passow and Carlson*, 2012]. The vertical transfer processes include passive sinking of organic particles, physical mixing of particulate and dissolved organic carbon (POC and DOC, respectively), and active transport by zooplankton migration. The amount of carbon taken up by photosynthesis depends partly on the size structure and taxonomic composition of phytoplankton, and the sinking of particles depends both on their size and chemical composition [*Armstrong et al.*, 2002; *Boyd and Newton*, 1999; *Guidi et al.*, 2009; *Lombard et al.*, 2013]. The POC flux decreases exponentially with depth as aggregates are fragmented, decomposed, and remineralized through respiration, and the carbon released in the water column above the depth of sequestration (defined below) returns to the atmosphere [*Martin et al.*, 1987]. It has been shown that a modest change in remineralization can have a substantial impact on atmospheric pCO_2; e.g., a deepening of the e-folding depth (i.e., the depth at which 63% of POC sinking from the surface waters is remineralized) by as little as ~20 m could lead to a decrease in atmospheric pCO_2 of 10 to 30 ppm, i.e., ~3 to 9% of the present atmospheric pCO_2 [*Kwon et al.*, 2009]. Furthermore, although POC remineralization is known to vary spatially in the oceans [*Buesseler et al.*, 2007], most global biogeochemical models that compute ocean carbon sequestration from sinking POC assume that remineralization is spatially uniform because its variability among ocean regions has not been adequately quantified. Hence, quantifying the ocean-wide variability of POC remineralization is of high priority to climate research.
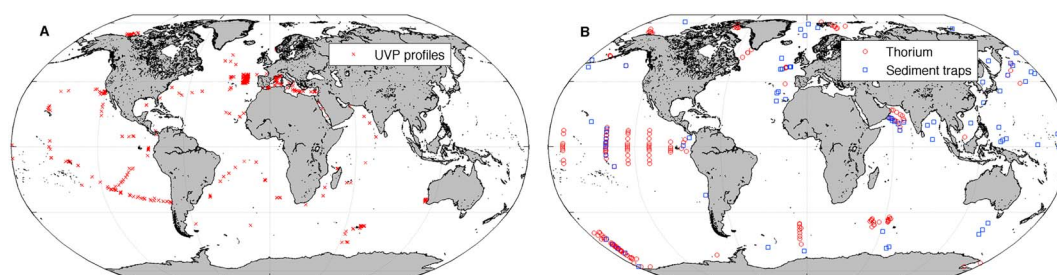
Figure 1. Locations of samples used in the present study. (a) UVP profiles. (b) The ^{234}Th/^{238}U disequilibrium and deep sediment traps.

Beside direct measurement of respiration [*Bendtsen et al.*, 2015], remineralization can be inferred from the vertical profile of particle flux through the water column. The vertical POC flux can be estimated at sea using a thorium isotope technique [*Buesseler et al.*, 2006], drifting sediment traps [*Boyd et al.*, 1999] deployed for a few hours or days, or from sediment traps moored at depths >1000 m [*Honjo et al.*, 2008]. One well-known example of remineralization derived from free-floating particle interceptor traps is found in *Martin et al.* [1987], who analyzed POC fluxes in traps deployed at eight stations in the northeast Pacific Ocean and one off Peru (depending on the sampling station, there were 9 to 25 traps within the range of sampled depths). The authors estimated the remineralization at each station by fitting a power law function to the POC flux profile. Using the same approach, *Berelson* [2001] estimated the remineralization in 17 data sets from U.S. Joint Global Ocean Flux Study (JGOFS) sites in the North Atlantic, the equatorial Pacific, the Arabian Sea, and the Southern Ocean. For each data set, the author first determined the average POC export at 100 m and then fitted the water column POC flux data with the equation of *Martin et al.* [1987]. So far, these labor-intensive methods have provided only a relatively small number of remineralization values for the world ocean.

In the present study, we develop a new approach to estimate and regionalize remineralization by combining ~2800 particle profiles from modern underwater imaging system with historical ~400 POC flux data from the thorium isotope method and ~150 deep sediment traps. Our regionalization approach is comparable to that developed earlier for photosynthetic parameters used for satellite-based estimation of primary production [*Platt et al.*, 1991; *Sathyendranath et al.*, 1995]. In our approach, we computed values of POC remineralization for each biogeochemical province of the global ocean [*Longhurst*, 1995]. Using our regionalized remineralization values together with POC export modeled from satellite data, we then calculated the carbon sequestration at both 2000 m and the depth of the top of the permanent pycnocline for each province and globally. We finally compared our new global estimates to values from the literature and discussed the potential biological processes governing the observed spatial variations in remineralization.

2. Material and Methods

2.1. Underwater Imaging System: The Underwater Vision Profiler

The Underwater Vision Profiler (UVP) was developed to quantify the vertical distributions of undisturbed large particles >100 μm in size in the water column [*Gorsky et al.*, 2000, 1992; *Picheral et al.*, 2010]. A main feature of the instrument is the recording of particle size distributions (PSDs) at a frequency comparable to that of physical (i.e., conductivity-temperature-depth), chemical, and optical sensors on a Rosette sampler. In this study, we used ~2800 PSD vertical profiles (binned in 5 m depth layers down to 1000 m depth on average) recorded throughout the world ocean since 1991 (Figure 1a), including those from the French JGOFS program and the Tara Oceans expedition [*Karsenti et al.*, 2011].

2.2. Particle Size-Based Carbon Flux Estimates

Previous research has shown that the distribution of particle size follows a *Junge*-type distribution over the micron to the millimeter size range [*Guidi et al.*, 2009; *McCave*, 1984; *Sheldon et al.*, 1972]. In theory, the carbon flux size-based approach relies on the use of that distribution and on the assumption that the total

Table 1. List of Symbols Used for Parameters and Variables and Their Dimensions (M for Mass, L for Length, and T for Time)

Symbol	Description	Dimensions
A	Constant for F	$ML^{(1-B)}T^{(-1)}$
B	Constant for F	-
b	Remineralization exponent	-
d	Particle diameter	L
F	Generic flux	$ML^{-2}T^{-1}$
F_{100}	Carbon flux (export) measured at 100 m	$ML^{-2}T^{-1}$
$F_{(z)}$	Carbon flux at depth (z)	$ML^{-2}T^{-1}$
F_{th}	Carbon flux (export) from disequilibrium between ^{238}U and ^{234}Th	$ML^{-2}T^{-1}$
F_{pyc}	Carbon flux (sequestration) at the top of the permanent pycnocline	$ML^{-2}T^{-1}$
F_s	Carbon flux (sequestration) from deep sediment traps	$ML^{-2}T^{-1}$
F_{2000}	Carbon flux (sequestration) at 2000 m or to the seafloor in pixels where water depth is between 200 and 2000 m	$ML^{-2}T^{-1}$
n	Particle number spectrum	L^{-4}
m	Particle mass	M
$S_{R(2000)}$	Regional sequestration at 2000 m	MT^{-1}
$S_{R(pyc)}$	Regional sequestration at the depth of the top of the permanent pycnocline	MT^{-1}
$\Sigma S_{(2000)}$	Global sequestration at 2000 m	MT^{-1}
$\Sigma S_{(pyc)}$	Global sequestration at the depth of the top of the permanent pycnocline	MT^{-1}
w	Particle settling rate	LT^{-1}
z	Depth	L
z_{th}	Depth of carbon flux (export) from disequilibrium between ^{238}U and ^{234}Th	L
z_s	Depth of carbon sequestration	L
σ_θ	Density value used to approximate the depth of the top of the permanent pycnocline	ML^{-3}

carbon flux of particles (F) corresponds to the flux spectrum integrated over all particle sizes from the smallest ($dmin$) to the largest ($dmax$) particle size:

$$F = \int_{dmin}^{dmax} n(d) \cdot m(d) \cdot w(d) \cdot \mathrm{d}d \tag{1}$$

where d is the particle diameter, $n(d)$ is the particle size spectrum, and $m(d)$ is the mass (here carbon content) of a spherical particle (see Table 1 for a summary of symbols).

In practice, the combined mass and settling rate of particles, $m(d)$ and $w(d)$, respectively, are often described as a power law function of their diameter obtained from a fit to particles collected by scuba divers [*Alldredge*, 1998; *Alldredge and Gotschalk*, 1988] or by comparing image-derived PSD with sediment traps estimate of mass flux [*Ebersbach et al.*, 2011; *Guidi et al.*, 2008; *Jouandet et al.*, 2011], giving $m(d) \cdot w(d) = Ad^B$, where A and B are the constants. Hence, the particle carbon flux can be approximated using equation (1) over a finite number of small logarithmic intervals for diameter d from 250 µm to 1.5 mm (particles <250 µm and >1.5 mm are not considered, as in *Guidi et al.* [2008], in order to use the fraction of the particle size spectrum that is coherent to all UVPs [*Guidi et al.*, 2009; *Picheral et al.*, 2010]), such that

$$F = \sum_{i=1}^{x} n_i A d_i^B \cdot d_i \tag{2}$$

where $A = 12.5 \pm 3.40 \, \text{mg m}^{1\text{-B}} \text{d}^{-1}$ and $B = 3.81 \pm 0.70$, corresponds to the best set of parameters that minimized the log-transformed differences between 118 sediment trap carbon flux estimates and UVP-recorded particle abundance and PSD [*Guidi et al.*, 2008].

2.3. Estimation of Remineralization Using Size-Based Carbon Flux Profiles

We obtained carbon flux profiles from UVP-recorded PSD profiles according to equation (2), after which we estimated remineralization by fitting the following power law function [*Martin et al.*, 1987] to the PSD-derived flux profiles:

$$F_{(z)} = F_{100}(z/100)^{-b} \tag{3}$$

where z is the depth and b is the remineralization exponent or efficiency at which the carbon exported from the upper ocean, here the POC flux at 100 m (F_{100}), decreases with depth. The F_{100} values derived from the UVP particle size distributions were not used in the remainder of the analysis. We finally calculated the

Spearman's correlation coefficient and corresponding P value between the modeled flux ($F_{(z)}$) and the PSD-derived flux in order to assess the quality of the fit. We only retained $b > 0$ calculated on profiles deeper than 500 m and showing a significant positive correlation between the model and the data ($P < 0.05$, one-tailed test).

2.4. Estimation of Remineralization Using Carbon Flux Estimates From ^{238}U/^{234}Th Disequilibrium and Deep Sediment Traps

We estimated remineralization by combining published databases providing estimates of the POC flux in deep sediment traps and carbon export from the upper ocean derived from water column measurements of disequilibrium between ^{238}U and ^{234}Th deposited on particles [*Henson et al.*, 2011; *Honjo et al.*, 2008] (Figure 1b). We partitioned the values in the two databases according to 56 ocean biogeographic provinces (Table S1 and Figure S1 in the supporting information) [*Longhurst*, 1995]. We calculated the remineralization exponent b for each province using all possible sets of carbon export (estimated from ^{238}U/^{234}Th disequilibrium, F_{th}) and carbon flux in the deep sediment traps (F_s) with the following equation, derived from equation (3):

$$F_s = F_{th}(z_s/z_{th})^{-b} \tag{4}$$

where z_s is the depth of the deep sediment traps, z_{th} is the depth of carbon export from disequilibrium between ^{238}U and ^{234}Th, and b is the remineralization exponent or efficiency at which the flux decreases between z_{th} and z_s.

2.5. Comparison of Remineralization Estimates

The above calculations provided, for each province, two sets of estimates of the remineralization exponent (b), i.e., values obtained from either size-based carbon flux profiles (equation (3)) or the method combining carbon fluxes from ^{238}U/^{234}Th disequilibrium and deep sediment traps (equation (4)). In order to decide if the two sets of estimates could be combined, we tested, using Mann-Whitney U tests, whether the b values from the two approaches belonged to the same statistical population. This test was performed for each biogeochemical province that simultaneously met the following conditions: it included ≥5 UVP profiles made during ≥2 different seasons and ≥5 remineralization estimates derived from ≥2 measurements of ^{238}U/^{234}Th disequilibrium and sediment traps. These conditions correspond to a compromise between maximizing the number of comparable provinces and comparing groups of b values representative of the annual range encountered in a given province.

2.6. Carbon Sequestration Estimates at the Regional and Global Scales

Carbon sequestration is often estimated from the carbon flux at 2000 m (F_{2000}; g C m^{-2} yr^{-1}) or to the seafloor when water depth is <2000 m and >200 m. F_{2000} is calculated using equation (3) with $z = 2000$. An alternative approach, implemented for the first time here, is to consider carbon as sequestered when it reaches the depth corresponding to the lower limit of the ventilated volume of the ocean [*Sarmiento and Toggweiler*, 1984], below which CO_2 is sequestered for a time that corresponds to that of the ocean's deep circulation (the average turnover time of the world ocean is about 1000 years [*Primeau*, 2005]). This depth is usually located near the top of the permanent pycnocline. According to *Sarmiento and Toggweiler* [1984], the depth of the ventilated volume (or hereinafter assimilated to the depth of the top of the permanent pycnocline) can be estimated using an empirical density value (σ_θ) at a global scale. In the present study, we selected $\sigma_\theta = 1027.6$ kg m^{-3} to approximate the depth of intermediate water masses and thus the top of the permanent pycnocline.

To quantify the depth of the top of the permanent pycnocline, we used the mean seasonal temperature and salinity from the World Ocean Atlas 2013 (http://www.nodc.noaa.gov/OC5/woa13/). These data sets cover the global ocean at a spatial resolution of 1°, with heterogeneous vertical resolution. For each grid cell, we calculated the values of temperature and salinity at every 10 m interval from surface to bottom using a spline interpolation. Then, we corrected for each season, depth and grid cell, the density values for the effect of hydrostatic pressure using the Seawater MATLAB© toolbox, and we retrieved the depth of top of the permanent pycnocline associated with the $\sigma_\theta = 1027.6$ kg m^{-3} isopycnal. In some specific areas, which were mainly located in high-latitude regions where a large part of the water column is

vertically mixed, the depth of the top of the permanent pycnocline could not retrieved, and we used instead the value of the maximum mixed-layer depth in the given geographical cell during the relevant season [*Montegut et al.*, 2004]. We calculated the annual mean depth of the top of the permanent pycnocline by averaging values computed for the four seasons. We obtained the POC carbon flux at the top of the permanent pycnocline (F_{pyc}) using equation (3) with $z = $ depth of the top of the permanent pycnocline.

In this study, estimates of carbon sequestration (S) were obtained by summing up POC flux values (F) over relevant surface areas. Hence, the dimensions of F are [$ML^{-2}T^{-1}$], and those of S are [MT^{-1}]. We estimated sequestration at 2000 m and at the top of the permanent pycnocline both at the regional scale of biogeochemical provinces [*Longhurst*, 1995] ($S_{R(2000)}$ or $S_{R(pyc)}$, Tg C yr^{-1}), by summing up POC flux values (F) in each pixel within the province, and at the global scale ($\Sigma S_{(2000)}$ or $\Sigma S_{(pyc)}$, Pg C yr^{-1}), adding up all regional sequestration values. We did not include in the calculation of sequestration estimates the pixels where water depth was <200 m.

2.7. Global Distribution of Phytoplankton Community Structure

In order to interpret spatial variations in flux attenuation, we compared our estimates with the structure of the phytoplankton communities in surface waters. For this purpose, we used the algorithm of *Uitz et al.* [2006], which infers the contribution of three phytoplankton size classes (microphytoplankton, $>20\,\mu m$; nanophytoplankton, 20 to $2\,\mu m$; and picophytoplankton, $<2\,\mu m$) to the total chlorophyll *a* concentration (Chl) from satellite-derived total surface Chl. In the present study, we used level 3 global area coverage Sea-viewing Wide Field-of-view Sensor monthly climatological data of surface Chl obtained for the time period of 1997–2010 or 1998–2010 depending on the month. The resulting monthly estimates were averaged to obtain annual estimates for each phytoplankton class in each biogeochemical province.

3. Results

3.1. Remineralization of POC, Carbon Flux at 2000 m, and Carbon Sequestration

Our approach to the estimation of the POC remineralization exponent (b), carbon flux at 2000 m (F_{2000}), and carbon sequestration ($S_{R(2000)}$ or $S_{R(pyc)}$ and $\Sigma S_{(2000)}$ or $\Sigma S_{(pyc)}$) proceeded in four successive steps. The first three steps were devoted to the estimation of b, which is the key parameter required to compute F_{2000}, $S_{R(2000)}$, $S_{R(pyc)}$, $\Sigma S_{(2000)}$, and $\Sigma S_{(pyc)}$.

First, we estimated b based on the global data set of F_s from deep sediment traps and an ocean-wide data set of F_{th} at 100 ± 20 m derived from water column measurements of disequilibrium between ^{238}U and ^{234}Th deposited on particles [*Henson et al.*, 2011; *Honjo et al.*, 2008] (Figure 1b). The horizontal distribution of observations is sparse (Figure 1b). In addition, the density of flux measurements is uneven among biogeochemical provinces, which is particularly true for the ^{234}Th flux measurements of which 75% were located in only 8 provinces (Table S2). We allocated the available F_s and F_{th} data to 18 ocean biogeographic provinces [*Longhurst*, 1995] (the remaining 38 provinces had no overlapping F_s and F_{th} data). Within each province, we applied equation (4) to all possible combinations of F_{th} estimates and F_s values. This produced 1971 b estimates, from which we calculated within-province medians (ranging from 0.64 to 1.82) and quartiles (Table S2).

Second, we determined b by fitting equation (3) to each vertical profile of carbon flux derived from UVP particle abundances and size distributions [*Guidi et al.*, 2008] (Figure 1a). Most of the UVP profiles were located between 40°S and 40°N, with ~40% of the data in the Mediterranean Sea (Figure 1a and Table S2). This spatial distribution of UVP records provided 897 b estimates in 20 provinces, from which we calculated within-province medians (ranging from 0.42 to 1.49) and quartiles (Table S2 and Data set S1 in the supporting information).

Third, among the 56 world ocean provinces, only 7 met all criteria allowing comparisons of b based on the two methods (see section 2.5). In each of the 7 testable provinces, the b values belonged to the same statistical population within that province (Mann-Whitney U tests, $P > 0.05$; Table S2 and Figure 2b, example using the South Pacific Subtropical Gyre province, SPSG). Given this result we grouped, within each province, the estimates of b from the two approaches and determined the median b. For each
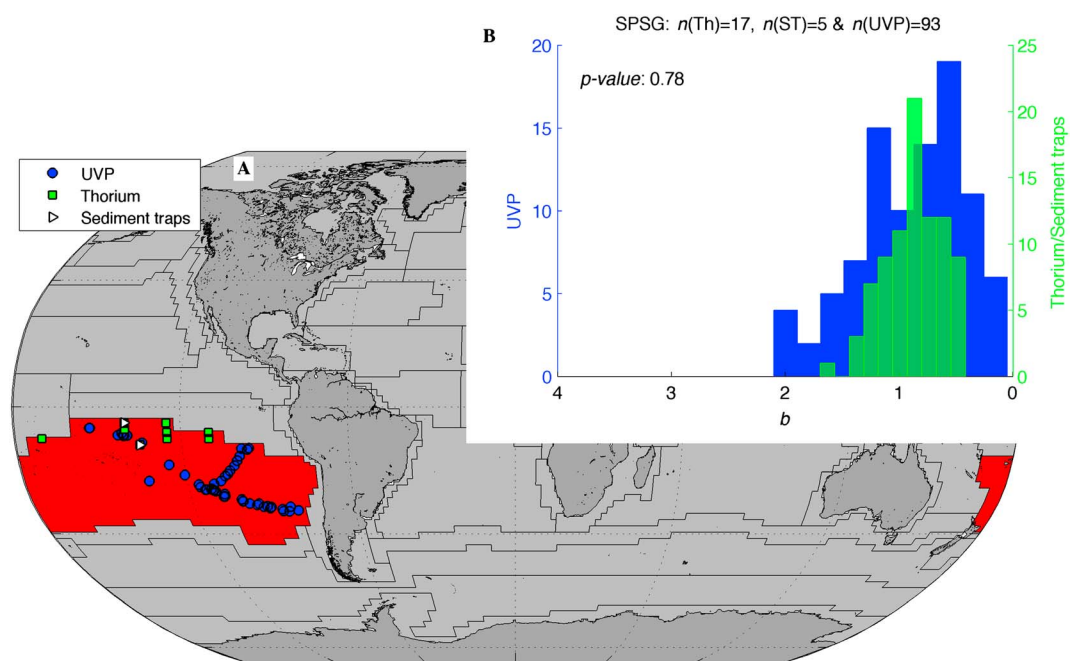
Figure 2. (a) Example of locations of ^{234}Th/^{238}U disequilibrium, deep sediment traps, and UVP profiles in the South Pacific Subtropical Gyre (SPSG). (b) Resulting distributions of b estimates calculated with equations (3) (UVP) and (4) (^{234}Th/^{238}U combined with deep sediment traps). The two distributions belonged to the same statistical population (Mann-Whitney U test, $P > 0.05$).

province where the number of b estimates was <5, b was set as the median of medians within the biome to which the province belonged (Table S1 for provinces and biomes). This way, we obtained one median b value (ranging from 0.42 to 1.75) for each of the 56 provinces (Table 2 and Figure 3b), with remineralization decreasing toward the equator and the lowest values being in the southern Indian Ocean.

Finally, using equation (3), we applied each regionalized b (Figure 3b) to carbon export estimates F_{100} (Figure 3a) to obtain the carbon flux at 2000 m (F_{2000}; Figure 3c) from which we calculated carbon sequestration ($S_{R(2000)}$ and $\Sigma S_{(2000)}$; Table 2). Figure 3c shows large variations of the carbon flux at 2000 m, with maximum values near the Subtropical Convergence, the Pacific Equatorial Divergence, and upwelling regions and minimum values in polar regions. It must be noted that carbon export estimates were previously validated against water column ^{234}Th data [*Henson et al.*, 2012] and are independent from the F_{100} values derived from the UVP particle profiles. We also estimated the carbon flux (Figure 3e) at the annual mean depth of the top of the permanent pycnocline (Figure 3d) from which we obtained alternative estimates of carbon sequestration ($S_{R(pyc)}$ or $\Sigma S_{(pyc)}$; Table 2). Figure 3d shows that this depth generally deepens toward the equator and is deeper in the Pacific than in the Atlantic Ocean.

We concluded this suite of calculations by examining the differences between the flux estimated at the depth of the top of the permanent pycnocline and at 2000 m (Figure 3f). The polar regions show large differences between the two estimates, corresponding to the shallowest values of the top of the permanent pycnocline (Figure 3d).

3.2. Spatial Variation of POC Remineralization, Carbon Flux at 2000 m, and Carbon Sequestration

In order to compare our regionalized b estimates to the b values modeled by *Henson et al.* [2012] for the world ocean, we recalculated regionalized b values from the latter. The ocean-wide distributions of these and our regionalized b values were quite similar, including the fact that 17 of the provinces where b was higher than the global median were the same in the two studies (Figures 4a and 4b and Table 2). In the present study, regional median b ranged between 0.42 and 1.75, and the global median b was 0.64 (Table 2). This range of 0.42 to 1.75 corresponds to −50 and +100% of the commonly used uniform $b = 0.86$.

Table 2. Comparison of F_{2000}, $S_{R(2000)}$, and $S_{R(pyc)}$ Obtained With Our New Approach (This Study), Using *Henson et al.* [2012], With Uniform $b = 0.86$, in the Different Biogeochemical Provinces [*Longhurst*, 1995][a]

Province	F_{2000} (g C m^{-2} yr^{-1})			$S_{R(2000)}$ (Tg C yr^{-1})			$S_{R(pyc)}$ (Tg C yr^{-1})	Remineralization (b)	
	This Study	Henson et al.	b = 0.86	This Study	Henson et al.	b = 0.86	This Study	This Study	Henson et al.
ALSK	6.14	1.93	4.11	2.90	0.93	1.92	3.31	0.64	0.85
ANTA	0.06	0.32	0.56	1.43	7.91	14.14	65.99	1.65	1.06
APLR	0.55	0.23	1.03	2.25	0.98	4.27	34.26	1.23	1.09
ARAB	2.20	4.44	1.21	6.72	13.51	3.70	8.03	0.64	0.37
ARCH	0.98	1.56	0.53	7.70	11.91	4.14	9.65	0.63	0.42
ARCT	0.33	1.15	1.98	1.09	4.34	6.85	131.20	1.75	0.93
AUSE	1.36	1.50	0.81	1.37	1.51	0.82	2.99	0.64	0.49
AUSW	2.74	2.05	0.96	7.07	4.98	2.46	7.65	0.42	0.48
BENG	6.39	3.56	4.36	7.00	3.88	4.79	6.61	0.64	0.64
BERS	3.72	1.76	4.10	9.16	4.46	10.12	11.55	0.91	0.92
BPLR	1.04	0.37	2.49	3.25	1.20	7.77	24.09	1.62	1.05
BRAZ	1.88	1.61	1.14	1.47	1.26	0.90	2.56	0.64	0.53
CAMR	2.66	3.91	1.67	2.79	4.15	1.74	2.79	0.64	0.38
CARB	1.64	2.13	0.77	5.74	7.37	2.70	7.87	0.55	0.40
CCAL	3.19	2.43	2.35	3.28	2.58	2.41	3.43	0.72	0.67
CHIL	2.48	3.42	2.33	7.15	9.37	6.72	7.26	0.83	0.65
CHIN	2.66	1.67	2.05	0.30	0.19	0.23	0.36	0.64	0.59
CNRY	6.30	8.44	3.57	2.63	3.50	1.48	3.16	0.64	0.48
EAFR	1.89	1.79	0.71	6.53	6.13	2.44	7.41	0.50	0.47
ETRA	1.57	2.95	0.78	8.41	15.65	4.18	11.48	0.63	0.42
FKLD	5.28	1.31	3.71	3.04	0.75	2.14	3.79	0.64	0.83
GFST	0.83	1.75	0.66	0.88	1.85	0.70	1.81	0.78	0.52
GUIA	1.75	2.33	1.14	1.05	1.37	0.69	1.39	0.64	0.38
GUIN	3.64	5.49	2.18	4.04	6.09	2.39	4.67	0.64	0.39
INDE	1.42	2.48	0.82	1.07	1.86	0.62	1.52	0.64	0.38
INDW	2.42	4.28	1.47	1.44	2.54	0.87	1.61	0.64	0.38
ISSG	1.40	1.17	0.41	26.49	21.83	7.83	29.44	0.45	0.50
KURO	1.44	1.71	1.00	5.00	5.99	3.48	5.97	0.73	0.57
MEDI	3.49	2.09	1.97	8.64	5.19	4.88	33.86	0.57	0.60
MONS	1.06	1.96	0.46	14.93	27.34	6.44	18.62	0.57	0.37
NADR	1.16	1.98	1.37	3.98	6.97	4.70	9.48	0.92	0.69
NASE	1.49	1.51	0.71	6.74	6.86	3.20	9.79	0.60	0.57
NASW	0.60	1.04	0.35	3.37	5.85	1.97	5.25	0.68	0.49
NATR	1.27	1.74	0.49	9.85	13.40	3.84	13.23	0.54	0.44
NECS	9.32	2.47	6.92	2.22	0.62	1.64	2.56	0.64	0.80
NEWZ	3.26	1.47	2.03	3.80	1.74	2.37	3.83	0.64	0.77
NPPF	1.25	1.40	0.99	4.37	4.91	3.47	4.95	0.78	0.74
NPSE	0.63	1.10	0.50	4.38	7.74	3.48	5.02	0.78	0.59
NPSW	0.50	1.22	0.39	1.86	4.56	1.47	2.11	0.78	0.47
NPTG	0.20	0.95	0.27	4.15	19.47	5.63	5.09	0.96	0.43
NWCS	6.35	2.06	4.61	8.16	2.81	5.90	12.92	0.64	0.74
OCAL	0.90	1.21	0.71	1.74	2.39	1.38	2.03	0.78	0.66
PEQD	1.15	2.13	0.70	11.54	21.39	7.02	13.43	0.69	0.48
PNEC	0.90	2.05	0.52	7.49	17.24	4.33	8.77	0.68	0.40
PSAE	1.46	1.26	1.30	4.20	3.64	3.73	5.11	0.82	0.87
PSAW	1.82	1.44	1.91	4.60	3.69	4.84	5.78	0.88	0.91
REDS	3.83	3.55	2.61	1.11	1.04	0.76	3.11	0.64	0.38
SANT	0.43	0.83	0.95	12.26	23.73	26.78	23.23	1.13	0.90
SARC	1.64	1.38	4.33	2.51	2.48	6.90	42.00	1.62	0.89
SATL	1.34	1.22	0.51	23.84	21.43	9.11	28.61	0.54	0.55
SPSG	0.38	1.00	0.36	13.81	35.46	13.16	16.46	0.84	0.52
SSTC	1.19	1.35	0.95	19.73	22.54	15.71	23.83	0.78	0.74
SUND	1.43	2.35	0.88	4.04	6.42	2.51	4.43	0.64	0.36
TASM	1.32	1.79	1.07	1.68	2.28	1.36	1.74	0.78	0.63
WARM	0.21	1.38	0.33	3.24	21.80	5.12	3.99	1.02	0.37
WTRA	1.08	2.12	0.54	5.67	11.10	2.84	8.20	0.63	0.40

Table 2. (continued)

Province	F_{2000} (g C m^{-2} yr^{-1})			$S_{R(2000)}$ (Tg C yr^{-1})			$S_{R(pyc)}$ (Tg C yr^{-1})	Remineralization (b)	
	This Study	Henson et al.	b = 0.86	This Study	Henson et al.	b = 0.86	This Study	This Study	Henson et al.
Global median	1.44	1.74	1.00	4.09	4.95	3.48	6.29	0.64	0.54
Minimum	0.06	0.23	0.27	0.30	0.19	0.23	0.36	0.42	0.36
Maximum	9.32	8.44	6.92	26.49	35.46	26.78	131.20	1.75	1.09
Number of >global median	27	29						26	27
Number of common[b]		20							17
$\Sigma S_{(2000)}$ (Pg C yr^{-1})				0.33	0.45	0.26			
$\Sigma S_{(pyc)}$ (Pg C yr^{-1})							0.72		

[a]In the last two columns, comparison of b per province obtained in this study where, for each province with a number of b estimates <5, b was set as the median of medians within the biome to which the province belonged (see Table S2 for provinces with b estimated from in situ data) and derived from *Henson et al.* [2012]. Finally, at the bottom of the table, global statistics, and $\Sigma S_{(2000)}$ and $\Sigma S_{(pyc)}$, the acronyms of biogeochemical provinces are defined in Table S1.
[b]Number of provinces either >median or ≤median in both columns.

The mean ocean b values in Table 2 are similar to the original value reported for the northeastern Pacific Ocean, i.e., 0.86 [*Martin et al.*, 1987], which is widely used in the literature to compute the deep POC fluxes (F_{2000}) and carbon sequestration ($S_{R(2000)}$ and $\Sigma S_{(2000)}$) from POC export (F_{100} or F_{th}) with equation (3). Doing so implicitly assumes that b is identical in all ocean provinces. However, values in Table 2 show that b is highly variable in space, i.e., the difference between the highest and the lowest b within each study ranges between 0.65 and 1.33 (e.g., $1.75 - 0.42 = 1.33$ for the present study). It follows that although the value b = 0.86 provides a useful reference at the global scale, it should not be used to accurately estimate POC fluxes and carbon sequestration at the regional scale.
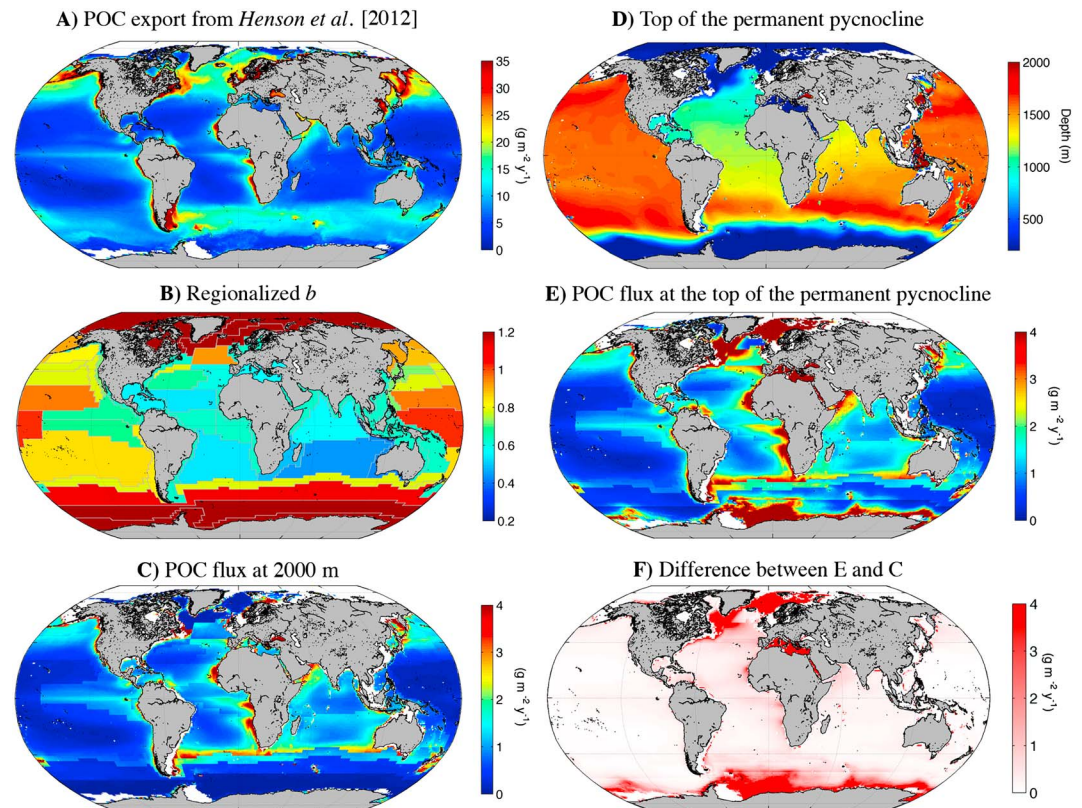

Figure 3. (a) POC export from the euphotic zone (F_{100}), from *Henson et al.* [2012]. (b) Regionalized estimates of mesopelagic remineralization b obtained in the present study. (c) POC flux at 2000 m or at the seafloor for water depths between 200 and 2000 m (F_{2000}). (d) Annual mean depth of the top of the permanent pycnocline, i.e., bottom depth of the ventilated water mass. (e) POC flux at the annual mean depth of the top of the permanent pycnocline (F_{pyc}). (f) Difference between POC flux at the annual mean depth of the top of the permanent pycnocline and at 2000 m (i.e., difference between Figures 3c and 3e).
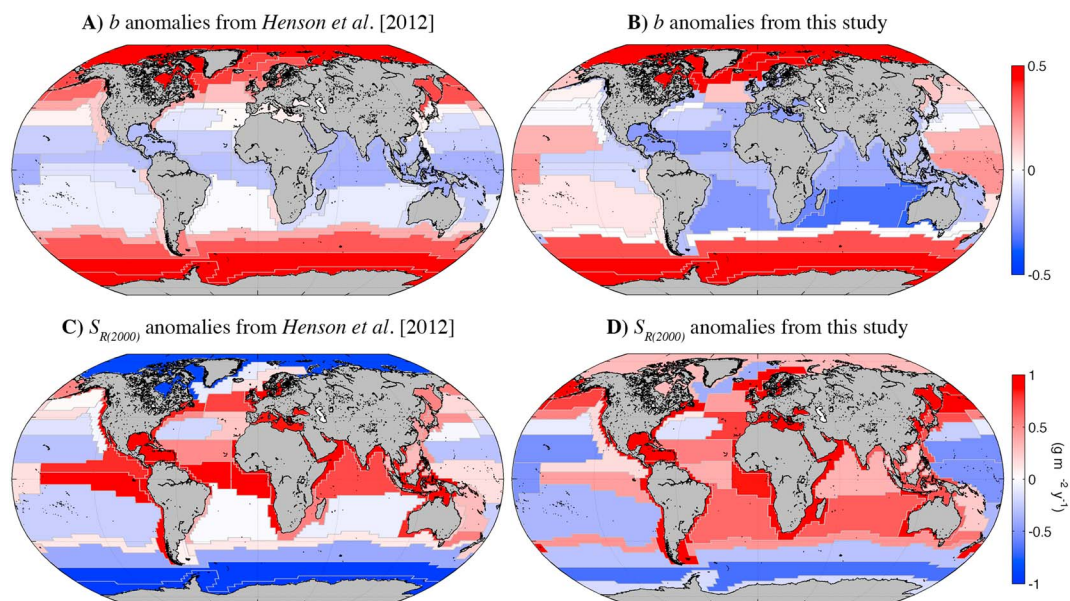
Figure 4. Distributions of b anomalies from the global mean: (a) from *Henson et al.* [2012] and (b) in the present study. Distributions of $S_{R(2000)}$ anomalies from the global median: (c) from *Henson et al.* [2012] and (d) in the present study. Data are provided in Table 2.

Our median F_{2000} value for the 56 provinces is 1.44 g C m^{-2} yr^{-1}, which is similar to the corresponding value of 1.74 g C m^{-2} yr^{-1} computed by *Henson et al.* [2012]. In addition, the horizontal patterns of our F_{2000} values in the world ocean are quite similar to those previously published [*Henson et al.*, 2012], including the fact that 20 of the provinces where median F_{2000} was higher than the global median were the same in the two studies (Figures 4c and 4d and Table 2). In Table 2, values of F_{2000} vary over more than 1 order of magnitude in each study, and most F_{2000} are ≤7 g C m^{-2} yr^{-1} in *Henson et al.* [2012], similar to our own values.

In order to compare our $\Sigma S_{(2000)}$ with values from previous studies we recalculated the global sequestration from *Henson et al.* [2012] according to the regionalized method presented here; i.e., we summed up the estimated $S_{R(2000)}$ for all biogeochemical provinces over all provinces using only pixel where bottom depth is >200 m. Our estimate of $\Sigma S_{(2000)}$ is 0.33 Pg C yr^{-1}, lower than the 0.45 Pg C yr^{-1} recalculated from *Henson et al.* [2012] (or 0.66 Pg C yr^{-1} in *Henson et al.*'s [2012] original study). This difference is explained by lower $S_{R(2000)}$ in 35 out of the 56 provinces (63%) in our study (Table 2). However, our lower $\Sigma S_{(2000)}$ is not due to uniformly lower $S_{R(2000)}$ values over these 35 provinces but instead to much lower $S_{R(2000)}$ values in a small number of provinces, i.e., 7 provinces accounted together for 78% of the difference in $\Sigma S_{(2000)}$ between the two studies. These provinces are located in warm waters of the Pacific (North Pacific Tropical Gyre, North Pacific Equatorial Countercurrent, Pacific Equatorial Divergence, Western Pacific Warm Pool, and South Pacific Subtropical Gyre) and Indian (Indian Monsoon Gyre) Oceans and in the Subantarctic Water Ring.

3.3. Effect of Variable b and Sequestration Depth

Several studies in the literature have estimated $\Sigma S_{(2000)}$ using equation (3) with $b = 0.86$ [*Martin et al.*, 1987] constant in space and time. The effect of using a uniform b instead of a spatially variable value, as proposed here and in a few other studies [*Henson et al.*, 2012; *Lutz et al.*, 2007], is illustrated by computing $\Sigma S_{(2000)}$ in the 56 ocean provinces using equation (3) with $b = 0.86$ and the regionalized F_{100} values from the present study. The $\Sigma S_{(2000)}$ that results from the calculation with uniform b is 0.26 Pg C yr^{-1}, which is 25% smaller than our estimate of 0.33 Pg C yr^{-1}. The overall difference of 0.08 Pg C yr^{-1} hides very large $S_{R(2000)}$ differences among provinces (Table 2); i.e., the $S_{R(2000)}$ values resulting from the uniform $b = 0.86$ approach are higher in polar provinces and lower in the Atlantic and Indian Oceans. In fact, the $S_{R(2000)}$ values computed with uniform $b = 0.86$ are smaller than those computed with our regionalized b values in 45 out of the 56 provinces (80%).
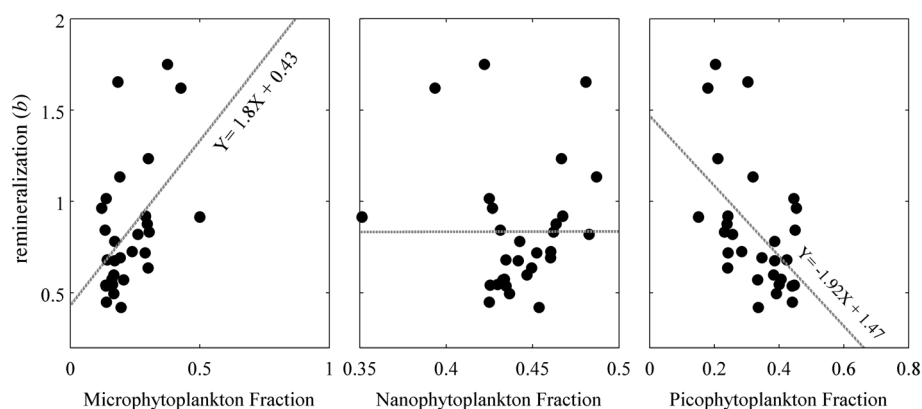
Figure 5. Scatters diagrams of median b values in different biogeochemical provinces [*Longhurst*, 1995] plotted as functions of the corresponding averaged fractions of microphytoplankton, nanophytoplankton, and picophytoplankton, respectively, in total phytoplankton chlorophyll biomass. Straight lines: ordinary least squares regressions of b on the three phytoplankton size fractions (Pearson's correlation coefficient for microphytoplankton $r = 0.48$, $P < 0.01$; nanophytoplankton $r = 0$, $P = 0.99$; and picophytoplankton $r = -0.51$, $P < 0.01$; two-tailed tests).

In addition, most published estimates of carbon sequestration have been calculated using a constant depth horizon (~2000 m, i.e., $\Sigma S_{(2000)}$). Here we found that sequestration calculated at the top of the pycnocline ($\Sigma S_{(pyc)}$) with our regionalized b values is equal to 0.72 Pg C yr^{-1}, which is more than twice the sequestration estimate calculated using our regionalized b values and the constant depth of 2000 m ($\Sigma S_{(2000)} = 0.33$ Pg C yr^{-1}; Table 2 and Figure 3f), and 3 times higher than the corresponding estimate calculated using $b = 0.86$ and constant depth of 2000 m ($\Sigma S_{(2000)} = 0.26$ Pg C yr^{-1}; Table 2). The difference in global sequestration between $\Sigma S_{(pyc)}$ and $\Sigma S_{(2000)}$, the two values being computed with regionalized b, hides very large differences between $S_{R(pyc)}$ and $S_{R(2000)}$ among provinces (Table 2), mostly in polar provinces (Figure 3f). Indeed, 73% of the difference between the two global sequestration estimates is due to differences in six polar provinces, i.e., Antarctic, Austral Polar, Atlantic Arctic, North Pacific Epicontinental, Boreal Polar, and Atlantic Subarctic (Table 2).

3.4. Relationship Between b and Phytoplankton Size Fractions

Figure 5 shows the scatters diagrams of b values in various biogeographic provinces plotted as a function of the corresponding Chl fraction of microphytoplankton, nanophytoplankton, or picophytoplankton, respectively. There were significant decreases of b with both a decrease in the fraction of larger phytoplankton ($r = 0.48$, $P < 0.01$) and an increase in the fraction of smaller phytoplankton ($r = -0.51$, $P < 0.01$). It must kept in mind that this relationship is strictly empirical and consequently does not imply a causal effect of the size structure of the phytoplankton assemblage on b.

4. Discussion

4.1. Novelty and Caveats of Our Approach

Our results show that the often-reported approach of using a uniform b value of 0.86 to compute F_{2000} with equation (3) leads to an underestimate of global carbon sequestration. Here we estimated b by fitting equation (3) to all possible combinations of water column F_{th} (i.e., the ^{234}Th-derived values in *Henson et al.* [2012]) and F_s from sediment traps [*Honjo et al.*, 2008] available within the same ocean province, resulting in 1971 b values. We combined these b values with 897 independent b estimates that we derived from vertical distributions of particles recorded with the UVP (total set of 1971 + 897 = 2868 b values), to obtain the largest data set on the remineralization exponent to date, from which we calculated median b values in the 56 ocean provinces. Finally, we used F_{100} from *Henson et al.* [2012] and our regionalized b values to calculate F_{2000} in the 56 ocean provinces. *Henson et al.* [2012] used 411 ^{234}Th-derived estimates of water column F_{th} (their Table S1) to validate their particulate export efficiencies (PE$_{eff}$ = F_{th}/PP) predicted by a previous algorithm [*Henson et al.*, 2011]. After validation, they computed F_{100} over the world ocean by multiplying satellite primary production (PP) [*Carr*, 2002] by PE$_{eff}$. Hence, our estimates of F_{2000} are not completely independent from previous published methods but linked to *Henson et al.* [2012] through ^{234}Th-derived water column estimates of F_{100}.

Table 3. Ocean Mean and Range of Values of Mesopelagic POC Remineralization (b), POC Flux at 2000 m (F_{2000}), and Sequestration at 2000 m ($\Sigma S_{(2000)}$) Reported by Different Authors and Estimated in the Present Study[a]

Study	Mean Ocean b Dimensionless	Range of b Dimensionless	Range of F_{2000} (g C m^{-2} yr^{-1})	$\Sigma S_{(2000)}$ (Pg C yr^{-1})
Martin et al. [1987]	0.86	0.32–0.97	0.8–7.0	0.12
Berelson [2001]	0.82	0.59–1.28	-	-
Lutz et al. [2007]	-	-	0.2–7	0.31
Honjo et al. [2008]	0.86	-	0.3–7.3	0.43
Henson et al. [2012]	0.64	0.24–1.18	0.0–35	0.66
This study	0.64[b]	0.42–1.75	0.1–9.3	0.33

[a](-): not applicable.
[b]Median value.

Each proposed approach to estimate b, F_{2000}, and $\Sigma S_{(2000)}$ has its own advantages and caveats. For example, approaches solely based on satellite variables produce estimates of global, spatially resolved flux and may include information on seasonal variability of PP [*Henson et al.*, 2012; *Lutz et al.*, 2007]. However, the validation of these estimates is difficult as in situ measurements are scarce. Conversely, our approach provides regionalized values of the remineralization exponent in biogeochemical provinces, but it does not account for seasonal variability as we merged space and time in order to maximize the number of potential b values per provinces. A main advantage of the present approach will be its ability to assimilate new water column values of b as they become available, which will be the case in coming years with the increase in vertical profiles of particles (e.g., UVP), whereas the number of sediment trap data will grow relatively slowly. In addition, imaging methods rely on the use of particle size distribution and concentration to estimate carbon flux assuming a power law relationship between sinking speed and particle size. However, variations sinking speed depend on changes not only in particle size [*Alldredge and Gotschalk*, 1988; *Guidi et al.*, 2008; *Iversen et al.*, 2010; *Jouandet et al.*, 2011] but also in composition and density [*Armstrong et al.*, 2002; *Francois et al.*, 2002; *McDonnell and Buesseler*, 2010]. Errors or spatial variations in the power law relationships would not affect estimates of b when changes with depth are small, but these estimates could be biased when sinking speed is greatly influenced by particle composition and density. Strikingly, the distributions of b estimates based on ^{234}Th/^{238}U combined with deep sediment traps and those from particulate profiles were comparable in all provinces where they could be statistically tested (Table S2 and Figure 2). This result suggests that particle size, rather than particle composition and density, drives the sinking speed of particle at the global scale. This could be further tested as the database allowing comparisons between the two methods becomes larger.

Finally, the depth of the bottom of the ventilated water mass was used to take into account the vertical and spatial variability in the depth of carbon sequestration [*Luyten et al.*, 1983]. Results show that taking into account this variability could lead to an ~120% increase in the total amount of carbon sequestered compared to sequestration at the classical 2000 m depth ($S_{R(pyc)}$ versus $S_{R(2000)}$; Table 2). This difference is mainly due to the inverse latitudinal gradients of the bottom depth of the ventilated water mass and POC export at that depth (Figures 3d and 3e). The method use here to compute is based on the empirical threshold $\sigma_\theta = 1027.6$, which is a compromise between values found in the literature [*Ledwell et al.*, 1993; *Sarmiento and Toggweiler*, 1984; *Sarmiento et al.*, 1988]. The bottom depth of the ventilated water mass could also be estimated using other approaches such as transient tracer age distributions or the Brunt-Väisälä frequency, but this is beyond the scope of the present study.

Overall, each estimate is regionalized, and each region corresponds to a specific ocean basin and specific biogeochemical and hydrodynamical characteristics [*Reygondeau et al.*, 2013]. Hence, b, F_{2000}, $S_{R(pyc)}$, and $S_{R(2000)}$ obtained in this study can potentially be used as references for regional studies assuming that biogeochemical processes are relatively uniform within a given province [*Longhurst*, 1995; *Reygondeau et al.*, 2013].

4.2. Comparison to Previous Estimates of Remineralization and Sequestration

Several estimates of b, F_{2000}, or $\Sigma S_{(2000)}$ can be found in the literature, based on different approaches. The published $\Sigma S_{(2000)}$ values range between 0.31 and 0.66 Pg C yr^{-1} (Table 3; excluding the earliest estimate of

0.12 Pg C yr^{-1} of *Martin et al.* [1987]). Comparing approaches used in previous studies provides information to understand the main sources of differences among them and to assess the potential of the approach proposed here for improving global sequestration estimates. The following paragraphs briefly summarize the previous approaches reported in Table 3.

In previous decades, *Martin et al.* [1987] and *Berelson* [2001] estimated *b* by fitting a power law function to POC flux measurements in free-floating or deep-moored sediment traps deployed at several depths and in a few locations and obtained average *b* estimates of 0.86 and 0.82, respectively. Although these two studies used an efficient approach to estimate the remineralization exponent and its temporal variability (*b* ranging from 0.32–0.97 to 0.59–1.28, respectively; Table 3), they did not provide enough values over the world ocean (i.e., 8 and 17 estimates of *b*, respectively) to assess its global variability.

Later, *Lutz et al.* [2007] assembled a data set of 244 annual flux estimates and 153 subannually resolved flux time series that they used to create POC flux climatologies. The objective was to predict the POC flux at 2000 m (F_{2000}) from satellite data. The authors first developed a seasonal variation index (SVI), using seasonally varying estimates of net primary production (NPP) derived from satellite data. Their algorithms described the remineralization of both labile and refractory fluxes as a function of sea surface temperature (SST) or NPP climatologies (satellite-derived rates and seasonal variability), using empirical relationships derived from sediment trap fluxes. The range of F_{2000} (0.2 to 7 g C m^{-2} yr^{-1}) in Table 3 was visually interpreted from the color map in Figure 14c of *Lutz et al.* [2007].

Similarly, *Honjo et al.* [2008] obtained a global sequestration estimate of 0.43 Pg C yr^{-1}, with F_{2000} ranging from 0.3 to 7.3 g C m^{-2} yr^{-1}, by summarizing the results from 153 time series sediment traps deployed in the world ocean between 1976 and 2004, of which 134 included full annual cycles. There were 32 traps deployed at 2000 m ± 5%, and the values of the other 121 traps (deployed between 1500 and 3500 m) were normalized to 2000 m using equation (3) with uniform $b = 0.87$. In order to geographically interpolate the water column-measured annual trap fluxes and calculate global mean fluxes, the authors developed four regional algorithms that correlated measured flux to modeled average annual primary production (PP) [*Behrenfeld and Falkowski*, 1997] and export production (EP) [*Laws et al.*, 2000] on a 250 × 250 km grid. The mean $b = 0.86$ presented in Table 3 was calculated, assuming that EP was equivalent to F_{100}, and the estimate of mean transfer efficiency (7.6%, TE = F_{2000}/EP) was used to compute $b = \log$ TE/$\log$ (2000/100) [*Francois et al.*, 2002].

More recently, *Henson et al.* [2012] published a study based on the 134 annual time series of POC flux at 2000 m from *Honjo et al.* [2008] (described above) combined with 411 [234]Th-derived estimates of POC export from the euphotic zone assembled from several publications. The authors showed that the best estimates of F_{2000} were obtained by combining a specific algorithm [*Carr*, 2002] to estimate NPP from satellite data and the SVI algorithm from *Lutz et al.* [2007] to estimate sequestration from seasonally varying NPP. The F_{2000} and $\Sigma S_{(2000)}$ values (0.0 to 35 gC m^{-2} yr^{-1} and 0.66 Pg C yr^{-1}, respectively) reported in Table 3 correspond to the carbon flux at 2000 m or to the seafloor in pixels where water depth is <2000 m for spatial variation of *b* ranging from 0.24 to 1.18.

The three above approaches [*Henson et al.*, 2012; *Honjo et al.*, 2008; *Lutz et al.*, 2007] use algorithms based on satellite climatologies of NPP and/or SST. Therefore, these approaches allow global estimates of F_{2000} or $\Sigma S_{(2000)}$; however, validation is difficult due to the limited number of POC export measurements and even more limited sediment trap time series measurement of deep POC fluxes, the latter being the only available reference for carbon sequestration to date. The relative paucity of available data causes uncertainties in the estimation of global POC fluxes and carbon sequestration and in the validation of estimates.

Overall, the temporal and spatial resolution of flux estimates provided by the previously published methods is too low to thoroughly validate/calibrate global biogeochemical models, such as those of *Lima et al.* [2014] and *Siegel et al.* [2014].

4.3. Why Does Remineralization Vary Spatially?

Flux attenuation in the mesopelagic layer is now known to vary spatially based on combinations of observations from sediment traps, [234]Th-derived fluxes, and satellite-derived primary production [*Berelson*, 2001;

Lam et al., 2011; *Lutz et al.*, 2007]. This spatial variability has been attributed to changes in the composition and distribution of communities of phytoplankton [*Boyd and Newton*, 1997; *Guidi et al.*, 2009] and zooplankton [*Banse*, 2013; *Fowler et al.*, 1987; *Steinberg et al.*, 2008] in the upper ocean. Indeed, the initial conditions of particle properties (i.e., size, composition, and porosity) are set in surface waters, which then influence their transit time through the water column. There, the activity of mesopelagic bacteria and zooplankton modifies the initial flux, either reducing its magnitude through particle remineralization, dissolution, and fragmentation or locally packaging small, nonsettling particles into larger, faster sinking ones [*Burd et al.*, 2010; *Robinson et al.*, 2010; *Stemmann et al.*, 2004].

Previous work, mostly based on local observations, has shown that in temperate productive regions, which are usually dominated by large phytoplankton [*Demarcq et al.*, 2012], the export flux of POC is substantial, but deep sequestration of the sinking POC is limited by the high flux attenuation in the mesopelagic layer [*Berelson*, 2001; *Guidi et al.*, 2009]. It was suggested that in such conditions, zooplankton may be the key players in remineralization, by preferentially feeding upon large, fast settling particles or breaking them down to smaller, slower settling particles [*Iversen et al.*, 2010; *Jackson and Checkley*, 2011]. Conversely, in tropical waters or the subtropical gyres, which are generally dominated by small cells, the export flux of POC is low, but flux attenuation in the mesopelagic layer (mostly caused by bacterial activity) is relatively weak allowing sequestration of a relatively high proportion of the exported POC [*Guidi et al.*, 2009; *Herndl and Reinthaler*, 2013]. These results suggest that there is a relationship between phytoplankton community structure in surface waters and *b* in the mesopelagic layer. Our novel ocean-wide database of regionalized *b* values combined with recent availability of global satellite-derived phytoplankton size classes [*Uitz et al.*, 2006] provided an opportunity to test this hypothesis on global scale.

The results illustrated in Figure 5 show that size structure of the phytoplankton assemblage and *b* are not independent in the present ocean. This provides a potential additional way for deriving mesopelagic *b* from satellite-derived information. Using the method of *Uitz et al.* [2006], one could compute the distribution of satellite-derived Chl among phytoplankton size classes and utilize the resulting values to estimate *b* using the linear multiple regression of the remineralization exponent (*b*) on the three phytoplankton size fractions:

$$b = 0.73F_{micro} + 0.70F_{nano} - 1.2F_{pico} + 0.76 \tag{5}$$

where F_{micro}, F_{nano}, and F_{pico} are the microphytoplanton, nanophytoplanton, and picophytoplanton fractions of total Chl. In the present ocean F_{micro} can vary between 0 and close to 1, whereas F_{pico} could accounts for 75% of total Chl at most [*Brewin et al.*, 2010; *Kostadinov et al.*, 2010; *Uitz et al.*, 2006, 2010]. Hence, equation (5) predicts that *b* would range between 0 and 1.4, which are realistic *b* values.

In addition, the relationship between phytoplankton community structure and *b* suggests a direction for future research. Indeed, the size and biodiversity of phytoplankton are predicted to decrease globally as the climate continues to change [*Finkel et al.*, 2010; *Passow and Carlson*, 2012; *Sommer and Lewandowska*, 2011]. For example, the contribution of microphytoplankton to the phytoplankton assemblage should decrease in the future ocean [*Bopp et al.*, 2005; *Cermeño et al.*, 2008], and that of smaller cells, such as coccolithophorids and picophytoplankton, should be less affected [*Cermeño et al.*, 2008; *Falkowski and Oliver*, 2007; *Li et al.*, 2009]. Although the relationships presented in Figure 5 and equation (5) are nonmechanistic and could even be spurious, if one assumed that the remineralization processes would not change under upcoming climate conditions and the relationships between the size structure of the phytoplankton community and *b* would hold, it could be speculated that there would be a general decrease in *b* at the global scale, with potential regional differences.

Another possible explanation for spatial variations in *b* could be variations in the biogeochemical environment though which a particle sinks. For example, the oxygen concentration in the mesopelagic water column can profoundly modify the structure of the zooplankton community and thus possibly reduce the flux attenuation under low-oxygen conditions [*Lima et al.*, 2014; *Robinson et al.*, 2010; *Roullier et al.*, 2014; *Van Mooy et al.*, 2002]. Consistent with this idea, our results show low-remineralization values in the North Indian and East equatorial Pacific Oceans, where there are intense oxygen minimum zones. However, this must be taken with caution because the low-remineralization values cited here are based on only few vertical UVP profiles.

5. Conclusion

We provide the first regionalized estimates of mesopelagic remineralization (*b*), which take full advantage of water column observations. We combine these remineralization estimates with satellite-derived estimates of export production and estimate global ocean carbon sequestration. Our value is 2 to 3 times higher than previous estimates using a globally uniform remineralization value and a constant depth (2000 m) for sequestration, which stresses the need to include regionally variable remineralization and sequestration depth for global estimates. Overall, the wide regional variability of *b* (between −50 and +100% of the standard value of *b* = 0.86 [*Martin et al.*, 1987]) precludes the use of globally uniform *b* in global biogeochemical models. We also have shown a strong statistical relationship at the global scale between mesopelagic *b* and the satellite-derived size structure of the phytoplankton assemblage in surface waters. The wide regional variability in *b* stresses the importance of using spatially variable values of organic carbon remineralization parameters to estimate or model the feedback of ocean carbon remineralization on atmospheric carbon.

References

Alldredge, A. (1998), The carbon, nitrogen and mass content of marine snow as a function of aggregate size, *Deep Sea Res., Part I, 45*(4–5), 529–541.

Alldredge, A. L., and C. Gotschalk (1988), In situ settling behavior of marine snow, *Limnol. Oceanogr., 33*(3), 339–351.

Armstrong, R. A., C. Lee, J. I. Hedges, S. Honjo, and S. G. Wakeham (2002), A new, mechanistic model for organic carbon fluxes in the ocean based on the quantitative association of POC with ballast minerals, *Deep Sea Res., Part II, 49*(1–3), 219–236.

Banse, K. (2013), Reflections about chance in my career, and on the top-down regulated world, *Annu. Rev. Mar. Sci., 5*, 1–19.

Behrenfeld, M. J., and P. G. Falkowski (1997), Photosynthetic rates derived from satellite-based chlorophyll concentration, *Limnol. Oceanogr., 42*(1), 1–20.

Bendtsen, J., K. M. Hilligsøe, J. L. S. Hansen, and K. Richardson (2015), Analysis of remineralisation, lability, temperature sensitivity and structural composition of organic matter from the upper ocean, *Prog. Oceanogr., 130*, 125–145, doi:10.1016/j.pocean.2014.10.009.

Berelson, W. M. (2001), The flux of particulate organic carbon into the ocean interior: A comparison of four U.S. JGOFS regional studies, *Oceanography, 14*, 59–67.

Bopp, L., O. Aumont, P. Cadule, S. Alvain, and M. Gehlen (2005), Response of diatoms distribution to global warming and potential implications: A global model study, *Geophys. Res. Lett., 32*, L19606, doi:10.1029/2005GL023653.

Boyd, P., and P. Newton (1997), Measuring biogenic carbon flux in the ocean, *Science, 275*(5299), 554–554.

Boyd, P. W., and P. P. Newton (1999), Does planktonic community structure determine downward particulate organic carbon flux in different oceanic provinces?, *Deep Sea Res., Part I, 46*(1), 63–91.

Boyd, P. W., et al. (1999), Transformations of biogenic particulates from the pelagic to the deep ocean realm, *Deep Sea Res., Part II, 46*(11–12), 2761–2792.

Brewin, R. J. W., S. Sathyendranath, T. Hirata, S. J. Lavender, R. M. Barciela, and N. J. Hardman-Mountford (2010), A three-component model of phytoplankton size class for the Atlantic Ocean, *Ecol. Model., 221*(11), 1472–1483, doi:10.1016/J.Ecolmodel.2010.02.014.

Buesseler, K. O., et al. (2006), An assessment of particulate organic carbon to thorium-234 ratios in the ocean and their impact on the application of Th-234 as a POC flux proxy, *Mar. Chem., 100*(3–4), 213–233.

Buesseler, K. O., et al. (2007), Revisiting carbon flux through the ocean's twilight zone, *Science, 316*(5824), 567–570, doi:10.1126/science.1137959.

Burd, A. B., et al. (2010), Assessing the apparent imbalance between geochemical and biochemical indicators of meso- and bathypelagic biological activity: What the @$#! is wrong with present calculations of carbon budgets?, *Deep Sea Res., Part II, 57*(16), 1557–1571, doi:10.1016/j.dsr2.2010.02.022.

Carr, M. E. (2002), Estimation of potential productivity in eastern boundary currents using remote sensing, *Deep Sea Res., Part II, 49*(1–3), 59–80, doi:10.1016/S0967-0645(01)00094-7.

Cermeño, P., S. Dutkiewicz, R. P. Harris, M. Follows, O. Schofield, and P. G. Falkowski (2008), The role of nutricline depth in regulating the ocean carbon cycle, *Proc. Natl. Acad. Sci. U.S.A., 105*(51), 20,344–20,349.

Demarcq, H., G. Reygondeau, S. Alvain, and V. Vantrepotte (2012), Monitoring marine phytoplankton seasonality from space, *Remote Sens. Environ., 117*, 211–222, doi:10.1016/J.Rse.2011.09.019.

Ebersbach, F., T. W. Trull, D. M. Davies, and S. G. Bray (2011), Controls on mesopelagic particle fluxes in the Sub-Antarctic and Polar Frontal Zones in the Southern Ocean south of Australia in summer—Perspectives from free-drifting sediment traps, *Deep Sea Res., Part II, 58*(21–22), 2260–2276.

Falkowski, P. G., and M. J. Oliver (2007), Mix and match: How climate selects phytoplankton, *Nat. Rev. Microbiol., 5*(10), 813–819.

Finkel, Z. V., J. Beardall, K. J. Flynn, A. Quigg, T. A. V. Rees, and J. A. Raven (2010), Phytoplankton in a changing world: Cell size and elemental stoichiometry, *J. Plankton Res., 32*(1), 119–137.

Fowler, S. W., P. Buat-Menard, Y. Yokoyama, S. Ballestra, E. Holm, and H. Van Nguyen (1987), Rapid removal of Chernobyl fallout from Mediterranean surface waters by biological activity, *Nature, 329*(6134), 56–58.

Francois, R., S. Honjo, R. Krishfield, and S. Manganini (2002), Factors controlling the flux of organic carbon to the bathypelagic zone of the ocean, *Global Biogeochem. Cycles, 16*(4), 1087, doi:10.1029/2001GB001722.

Gorsky, G., C. Aldorf, M. Kage, M. Picheral, Y. Garcia, and J. Favole (1992), Vertical distribution of suspended aggregates determined by a new Underwater Video Profiler, paper presented at 3ème Colloque du Programme National sur le Determinisme du Recrutement, Nantes (France), Annales de l'Institut oceanographique, Paris, Nantes (France), 1–3 Oct. 1991.

Gorsky, G., M. Picheral, and L. Stemmann (2000), Use of the Underwater Video Profiler for the study of aggregate dynamics in the North Mediterranean, *Estuarine Coastal Shelf Sci., 50*(1), 121–128.

Guidi, L., G. A. Jackson, L. Stemmann, J. C. Miquel, M. Picheral, and G. Gorsky (2008), Relationship between particle size distribution and flux in the mesopelagic zone, *Deep Sea Res., Part I, 55*, 1364–1374, doi:10.1016/j.dsr.2008.05.014.

Guidi, L., L. Stemmann, G. A. Jackson, F. Ibanez, H. Claustre, L. Legendre, M. Picheral, and G. Gorsky (2009), Effects of phytoplankton community on production, size, and export of large aggregates: A world-ocean analysis, *Limnol. Oceanogr.*, *54*(6), 1951–1963.

Henson, S. A., R. Sanders, E. Madsen, P. J. Morris, F. Le Moigne, and G. D. Quartly (2011), A reduced estimate of the strength of the ocean's biological carbon pump, *Geophys. Res. Lett.*, *38*, L04606, doi:10.1029/2011GL046735.

Henson, S. A., R. Sanders, and E. Madsen (2012), Global patterns in efficiency of particulate organic carbon export and transfer to the deep ocean, *Global Biogeochem. Cycles*, *26*, GB1028, doi:10.1029/2011GB004099.

Herndl, G. J., and T. Reinthaler (2013), Microbial control of the dark end of the biological pump, *Nat. Geosci.*, *6*(9), 718–724.

Honjo, S., S. J. Manganini, R. A. Krishfield, and R. Francois (2008), Particulate organic carbon fluxes to the ocean interior and factors controlling the biological pump: A synthesis of global sediment trap programs since 1983, *Prog. Oceanogr.*, *76*(3), 217–285, doi:10.1016/j.pocean.2007.11.003.

Iversen, M. H., N. Nowald, H. Ploug, G. A. Jackson, and G. Fischer (2010), High resolution profiles of vertical particulate organic matter export off Cape Blanc, Mauritania: Degradation processes and ballasting effects, *Deep Sea Res., Part I*, *57*(6), 771–784, doi:10.1016/j.dsr.2010.03.007.

Jackson, G. A., and D. M. Checkley (2011), Particle size distributions in the upper 100 m water column and their implications for animal feeding in the plankton, *Deep Sea Res., Part I*, *58*(3), 283–297, doi:10.1016/J.Dsr.2010.12.008.

Jouandet, M.-P., T. W. Trull, L. Guidi, M. Picheral, F. Ebersbach, L. Stemmann, and S. Blain (2011), Optical imaging of mesopelagic particles indicates deep carbon flux beneath a natural iron-fertilized bloom in the Southern Ocean, *Limnol. Oceanogr.*, *56*(3), 1130–1140.

Karsenti, E., et al. (2011), A holistic approach to marine eco-systems biology, *Plos Biol.*, *9*(10), doi:10.1371/journal.pbio.1001177.

Kostadinov, T. S., D. A. Siegel, and S. Maritorena (2010), Global variability of phytoplankton functional types from space: Assessment via the particle size distribution, *Biogeosciences*, *7*(10), 3239–3257, doi:10.5194/bg-7-3239-2010.

Kwon, E. Y., F. Primeau, and J. L. Sarmiento (2009), The impact of remineralization depth on the air-sea carbon balance, *Nat. Geosci.*, *2*(9), 630–635.

Lam, P. J., S. C. Doney, and J. K. B. Bishop (2011), The dynamic ocean biological pump: Insights from a global compilation of particulate organic carbon, CaCO(3), and opal concentration profiles from the mesopelagic, *Global Biogeochem. Cycles*, *25*, GB3009, doi:10.1029/2010GB003868.

Lampitt, R. S., et al. (2008), Ocean fertilization: A potential means of geoengineering?, *Philos. Trans. R. Soc. London, Ser. A*, *366*(1882), 3919–3945.

Laws, E. A., P. G. Falkowski, W. O. Smith, H. Ducklow, and J. J. McCarthy (2000), Temperature effects on export production in the open ocean, *Global Biogeochem. Cycles*, *14*(4), 1231–1246, doi:10.1029/1999GB001229.

Ledwell, J. R., A. J. Watson, and C. S. Law (1993), Evidence for slow mixing across the pycnocline from an open-ocean tracer-release experiment, *Nature*, *364*(6439), 701–703, doi:10.1038/364701a0.

Li, W. K. W., F. A. McLaughlin, C. Lovejoy, and E. C. Carmack (2009), Smallest algae thrive as the Arctic Ocean freshens, *Science*, *326*(5952), 539–539, doi:10.1126/Science.1179798.

Lima, I. D., P. J. Lam, and S. C. Doney (2014), Dynamics of particulate organic carbon flux in a global ocean model, *Biogeosciences*, *11*(4), 1177–1198.

Lombard, F., L. Guidi, and T. Kiørboe (2013), Effect of type and concentration of ballasting particles on sinking rate of marine snow produced by the appendicularian *Oikopleura dioica*, *PLoS One*, *8*(9), e75676, doi:10.1371/journal.pone.0075676.

Longhurst, A. R. (1995), Seasonal cycles of pelagic production and consumption, *Prog. Oceanogr.*, *36*(2), 77–167.

Lutz, M. J., K. Caldeira, R. B. Dunbar, and M. J. Behrenfeld (2007), Seasonal rhythms of net primary production and particulate organic carbon flux to depth describe the efficiency of biological pump in the global ocean, *J. Geophys. Res.*, *112*, C10011, doi:10.1029/2006JC003706.

Luyten, J. R., J. Pedlosky, and H. Stommel (1983), The ventilated thermocline, *J. Phys. Oceanogr.*, *13*(2), 292–309, doi:10.1175/1520-0485(1983)013<0292:Tvt>2.0.Co;2.

Martin, J. H., G. A. Knauer, D. M. Karl, and W. W. Broenkow (1987), VERTEX: Carbon cycling in the northeast Pacific, *Deep Sea Res. A*, *34*(2A), 267–285.

McCave, I. N. (1984), Size spectra and aggregation of suspended particles in the deep ocean, *Deep Sea Res., Part I*, *31*(4), 329–352.

McDonnell, A. M. P., and K. O. Buesseler (2010), Variability in the average sinking velocities of marine particles, *Limnol. Oceanogr.*, *55*(5), 2085–2096, doi:10.4319/lo.2010.55.5.2085.

Montegut, C. D., G. Madec, A. S. Fischer, A. Lazar, and D. Iudicone (2004), Mixed layer depth over the global ocean: An examination of profile data and a profile-based climatology, *J. Geophys. Res.*, *109*, C12003, doi:10.1029/2004JC002378.

Passow, U., and C. A. Carlson (2012), The biological pump in a high CO_2 world, *Mar. Ecol. Prog. Ser.*, *470*, 249–271, doi:10.3354/meps09985.

Picheral, M., L. Guidi, L. Stemmann, D. M. Karl, G. Iddaoud, and G. Gorsky (2010), The Underwater Vision Profiler 5: An advanced instrument for high spatial resolution studies of particle size spectra and zooplankton, *Limnol. Oceanogr. Meth.*, *8*, 462–473, doi:10.4319/lom.2010.8.462.

Platt, T., C. Caverhill, and S. Sathyendranath (1991), Basin-scale estimates of oceanic primary production by remote sensing: The North Atlantic, *J. Geophys. Res.*, *96*(C8), 15,147–15,159, doi:10.1029/91JC01118.

Primeau, F. (2005), Characterizing transport between the surface mixed layer and the ocean interior with a forward and adjoint global ocean transport model, *J. Phys. Oceanogr.*, *35*(4), 545–564, doi:10.1175/Jpo2699.1.

Reygondeau, G., A. Longhurst, E. Martinez, G. Beaugrand, D. Antoine, and O. Maury (2013), Dynamic biogeochemical provinces in the global ocean, *Global Biogeochem. Cycles*, *27*, 1046–1058, doi:10.1002/Gbc.20089.

Robinson, C., et al. (2010), Mesopelagic zone ecology and biogeochemistry—A synthesis, *Deep Sea Res., Part II*, *57*(16), 1504–1518, doi:10.1016/j.dsr2.2010.02.018.

Roullier, F., L. Berline, L. Guidi, X. Durrieu De Madron, M. Picheral, A. Sciandra, S. Pesant, and L. Stemmann (2014), Particle size distribution and estimated carbon flux across the Arabian Sea oxygen minimum zone, *Biogeosciences*, *11*(16), 4541–4557, doi:10.5194/bg-11-4541-2014.

Sarmiento, J. L., and J. R. Toggweiler (1984), A new model for the role of the oceans in determining atmospheric pCO_2$, *Nature*, *308*(5960), 621–624, doi:10.1038/308621a0.

Sarmiento, J. L., J. R. Toggweiler, and R. Najjar (1988), Ocean carbon-cycle dynamics and atmospheric pCO_2$, *Philos. Trans. R. Soc., A*, *325*(1583), 3–21, doi:10.1098/Rsta.1988.0039.

Sathyendranath, S., A. Longhurst, C. M. Caverhill, and T. Platt (1995), Regionally and seasonally differentiated primary production in the North Atlantic, *Deep Sea Res., Part I*, *42*(10), 1773–1802.

Sheldon, R. W., A. Prakash, and W. H. Sutcliff (1972), Size distribution of particles in ocean, *Limnol. Oceanogr.*, *17*(3), 327–340.

Siegel, D. A., K. O. Buesseler, S. C. Doney, S. F. Sailley, M. J. Behrenfeld, and P. W. Boyd (2014), Global assessment of ocean carbon export by combining satellite observations and food-web models, *Global Biogeochem. Cycles*, *28*, 181–196, doi:10.1002/2013GB004743.

Sommer, U., and A. Lewandowska (2011), Climate change and the phytoplankton spring bloom: Warming and overwintering zooplankton have similar effects on phytoplankton, *Global Change Biol.*, *17*(1), 154–162, doi:10.1111/J.1365-2486.2010.02182.X.

Steinberg, D. K., B. A. S. Van Mooy, K. O. Buesseler, P. W. Boyd, T. Kobari, and D. M. Karl (2008), Bacterial vs. zooplankton control of sinking particle flux in the ocean's twilight zone, *Limnol. Oceanogr.*, *53*(4), 1327–1338.

Stemmann, L., G. A. Jackson, and G. Gorsky (2004), A vertical model of particle size distributions and fluxes in the midwater column that includes biological and physical processes—Part II: Application to a three year survey in the NW Mediterranean Sea, *Deep Sea Res., Part I*, *51*(7), 885–908.

Uitz, J., H. Claustre, A. Morel, and S. B. Hooker (2006), Vertical distribution of phytoplankton communities in open ocean: An assessment based on surface chlorophyll, *J. Geophys. Res.*, *111*, C08005, doi:10.1029/2005JC003207.

Uitz, J., H. Claustre, B. Gentili, and D. Stramski (2010), Phytoplankton class-specific primary production in the world's oceans: Seasonal and interannual variability from satellite observations, *Global Biogeochem. Cycles*, *24*, GB3016, doi:10.1029/2009GB003680.

Van Mooy, B. A. S., R. G. Keil, and A. H. Devol (2002), Impact of suboxia on sinking particulate organic carbon: Enhanced carbon flux and preferential degradation of amino acids via denitrification, *Geochim. Cosmochim. Acta*, *66*(3), 457–465, doi:10.1016/S0016-7037(01)00787-6.